21th Annual CFD Symposium,
August 8-9, 2019, Bangalore

ANSYS MOSAIC POLY-HEXCORE MESH FOR HIGH-LIFT AIRCRAFT CONFIGURATION

Krishna Zore[1]
(krishna.zore@ansys.com)
ANSYS, Inc
Plot no. 34/1, Hinjewadi, Pune-411057,
Maharashtra, India

Balasubramanyam Sasanapuri[3]
(balasubramanyam.sasanapuri@ansys.com)
ANSYS, Inc
Unit no. 906, The Platina, Gachibowli, Hyderabad-500032, Telangana, India

Gandhar Parkhi[2]
(gandhar.parkhi @ansys.com)
ANSYS, Inc
Plot no. 34/1, Hinjewadi, Pune-411057,
Maharashtra, India

Alan Varghese[4]
(alan.varghese @ansys.com)
ANSYS, Inc
Plot no. 34/1, Hinjewadi, Pune-411057,
Maharashtra, India

ABSTRACT

ANSYS Fluent Mosaic™ meshing technology connects any type of mesh element to any other type of element automatically and conformally. The Poly-Hexcore, first application of the Mosaic technology connects high-quality octree hexahedron in the bulk region, and isotropic poly-prisms in the boundary layer with the Mosaic polyhedral elements. This results in an approximately *20* to *50%* reduction in the total element count compared to the conventional Hexcore mesh. That consequently speeds up the ANSYS Fluent solver by *10* to *50%* depending upon the application. So, to verify the solver speedup and accuracy in predicting complex high-lift aerodynamics, a typical 100-passenger class regional jet airliner in a nominal landing configuration is chosen from the NASA 3rd AIAA CFD High-Lift Prediction Workshop[1]. ANSYS Fluent R19.2, a cell-centered Reynolds-Averaged Navier-Stokes CFD solver, with Shear Stress Transport (SST k-ω) and Transition-SST (γ-Reθ) turbulence model are used to obtain the computational results. The Mosaic Poly-Hexcore mesh with *~48%* reduction in the total element count produces similar results compared to the conventional Hexcore mesh, with *~41%* less computational time. Further, the accuracy of computational results obtained from both the meshes are confirmed by comparing aerodynamic force coefficients, wing spanwise pressure coefficient, surface oil flow and china-clay visualizations with the wind tunnel measurement data.

Key words: Mosaic, Polyhedral, Aerodynamics, Turbulent, CFD

NOMENCLATURE

JSM	=	JAXA Standard Model
WBNP	=	Wing-Body-Nacelle-Pylon
JAXA	=	Japan Aerospace Exploration Agency
CFD	=	Computational Fluid Dynamics
FTF	=	Flap Track Fairing
c	=	Chord Length
C_p	=	Pressure Coefficient
α	=	Angle of Attack
C_L	=	Lift Coefficient
C_D	=	Drag Coefficient
C_M	=	Moment Coefficient
TS	=	Tollmien-Schlichting instability
CF	=	Crossflow instability
CAD	=	Computer Aided Design
MAC	=	Mean Aerodynamic Chord
Re	=	Reynolds Number
γ	=	Turbulence Intermittency
Reθ	=	Momentum thickness Reynolds number

INTRODUCTION

Aircrafts in a nominal take-off/landing configuration with high-lift devices deployed results in a set of flow complexities, such as laminar-turbulent transition, strong adverse pressure gradients, wake-boundary layer interactions, streamlines curvature and an increase in wingtip vortices strength[2-7]. Furthermore, support brackets, engine nacelle-pylon interaction with high lift devices and the gap between the inner slat end and fuselage alters the flow behavior in a nontrivial way[2,6], which further complicates the overall flow behavior.

Thus, the complex nature of the resulting flow fields and the uncertainties in locating onset transition makes it very difficult for conventional computational fluid dynamics (CFD) modeling approaches to accurately predict aerodynamic forces on high-lift configurations. However, understanding of the detailed flow physics is paramount and thus requires efficient and accurate mesh preparation, so that high-fidelity simulations can be performed in a computationally tractable time.

Therefore, in this paper, we use the novel ANSYS Fluent Mosaic™ meshing technology to generate efficient, high-quality meshes using Poly-Hexcore topology, which provides novel meshing strategies to solve flow around increasingly complex geometries with greater accuracy and speed. In general, this technology conformally connects various types of meshes with general polyhedral elements automatically. Here, the new Poly-Hexcore feature in ANSYS Fluent uses this Mosaic™ technology to fill the bulk region with octree hexahedral elements, maintain high-quality, layered isotropic poly-prisms in the boundary layer and conformally connects them with the generalized polyhedral elements. Such Poly-Hexcore meshes promise to yield reduced mesh count, higher mesh quality, and better solver performance when compared with other conventional meshing technologies.

This validation study demonstrates the advantages of Mosaic-enabled unstructured meshing for steady RANS simulations on the JAXA Standard Model (JSM)[1] with engine nacelle-pylon, a representative of a typical 100-passenger class regional jet airliner. The model was tested in *6.5m x 5.5m* JAXA- Low Speed Wind Tunnel (LWT1)[6], and the CAD geometry, flow operating conditions and experimental data was supplied by NASA's 3rd AIAA CFD High Lift Prediction Workshop[1] committee. The detailed workshop test cases study performed by ANSYS participation using committee supplied BETA-CAE ANSA and Pointwise® meshes can be found in the reference 2. Similarly, the test Case-2 JSM (without nacelle-pylon) validation study, prepared with ANSYS Fluent R18.2 unstructured prism-tetrahedron mesh, can be found in reference 3.

MOSAIC MESHING TECHNOLOGY

Mosiac™ meshing is an innovative ANSYS Fluent meshing technology which automatically, conformally combines a boundary layer meshes using high-quality polyhedron to hexahedron elements in the bulk region[9]. Figure 1 shows the first application of the Mosaic technology, the Poly-Hexcore, wherein the bulk region is filled with octree hexahedral elements *(blue color)*, the boundary layer is filled with isotropic poly-prisms *(orange color)* and the transition is filled with Mosaic polyhedral elements *(lime green color)*. In the future, this technology will allow Mosaic polyhedron elements to connect with any surface (triangles, quad, polygon) and volume (hexahedron, tetrahedron, pyramid, wedge-prism) elements. The Mosaic meshing in ANSYS Fluent follows a "Bottom-Up" volume mesh generation approach, contrary to some of the other meshing techniques, which follow a "Top-Down" approach. The "Bottom-Up" approach provides freedom to generate high quality thick prism layers, while respecting geometric fidelity, which is very challenging in cartesian based cut/snapped "Top-Down" meshing approaches.

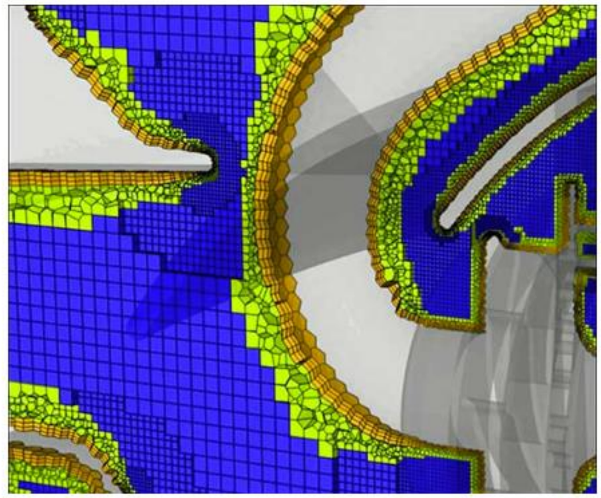

Figure 1. Mosaic Poly-Hexcore mesh.

Furthermore, this technology is parallel scalable on high-performance computing *(HPC)* platforms and lead to quicker mesh generation. For example, on a multi-core machine *(CPU: 2x Intel(R) Xeon(R) Gold 6142 CPU @ 2.60GHz, RAM: 192GB (6GB/core)),* creating a *100* million element mesh is *~6* times faster, when scaled from the serial compute core to *32* parallel compute cores. Additionally, the Mosaic meshing leads to *20 - 50%* reduction in the total element count compared to the conventional Hexcore meshing. Which consequently speeds up the ANSYS Fluent solver by *10 - 50%,* giving similar results and consuming less machine memory. This technology was also validated on an automotive application, the generic DrivAer car model to predict complex vehicle aerodynamic phenomenona[8].

MODEL DESCRIPTION AND MESH DETAILS

The JSM with support brackets (such as the slat tracks and the flap track fairings *(FTFs)*) and nacelle/pylon-on, in nominal landing configuration with slats and flaps deployed at 30^0 is shown in Figure 2. The geometric parameters of the scaled model are shown in Table 1.

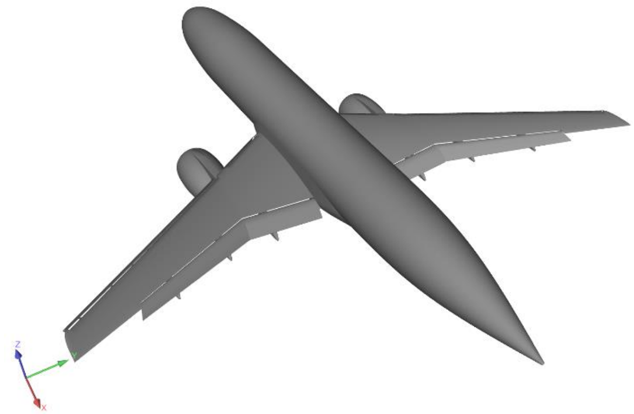

Figure 2. JSM-WBNP CAD Geometry.

Table 1. JSM-WBNP Geometric parameters.

Geometric parameters	**Units**
Mean aerodynamic chord (MCA)	529.2 mm **model scale**
Wing semi-span	2300.0 mm
Reference area of the semi-span model ($S_{ref}/2$)	1123300.0 mm^2
Moment reference center (MRC)	X = 2375.7 mm, y = 0.0 mm, z = 0.0 mm

The CAD geometry in the IGES-file format is taken from the NASA AIAA 3rd CFD High-Lift Prediction Workshop[1]. Minor CAD repairs, watertight box-shaped flow domain and the wake refinement Bodies of Influences (BOIs) are prepared using ANSYS multi-purpose 3D Discovery SpaceClaim CAD modeler. However, the local mesh refinement offset BOIs around the fuselage, wing, slat, flap, nacelle-pylon and support brackets are automatically prepared within ANSYS Fluent meshing tool, using an offset method, which smartly scales the selected surfaces according to the user input offset distance. Figure 3 shows the box-shaped farfield flow domain and the BOIs refinement regions.

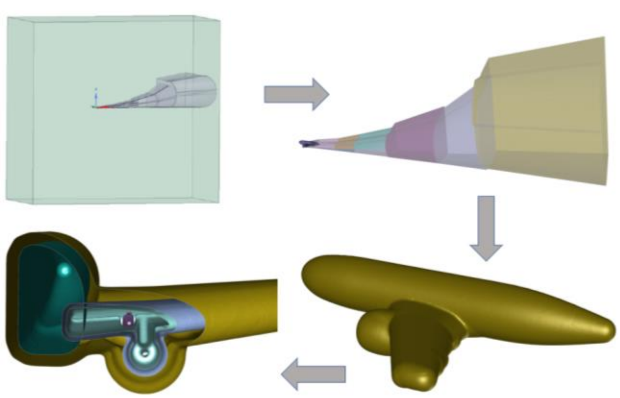

Figure 3. JSM, farfield domain, and BOI (refinement) regions.

The high-quality triangular surface mesh is prepared within ANSYS Fluent's meshing tool. Scoped sizing functionality is used to define surface zone sizes, based on the curvature, proximity and soft size requirements. This surface mesh is used to generate Hexcore and Mosaic Poly-Hexcore volume meshes. However, for the Mosaic Poly-hexcore process, the surface mesh is converted to polys, by maintaining average edge length consistency with the triangular surface mesh. Figure 4a. shows the triangular surface mesh used to generate the Hexcore volume mesh, and Figure 4b. shows the poly surface mesh converted during the Mosaic Poly-Hexcore generation.

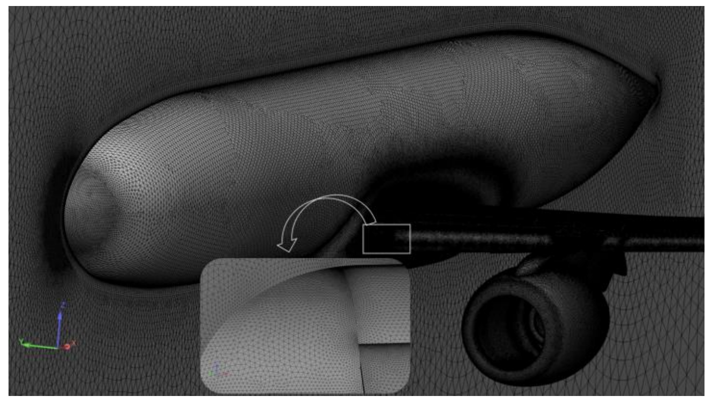

(a)

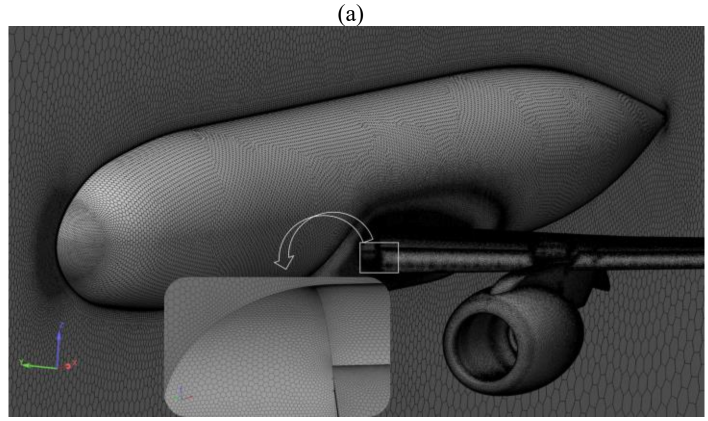

(b)

Figure 4. JSM-WBNP, Surface mesh, (a) Hexcore, (b) Mosaic Poly-Hexcore.

Figure 5 shows a combined image of the surface and the volume mesh on the cut plane intersecting the wing and the flap. The Hexcore mesh with surface triangles, wedge-prism, transition tetrahedron and bulk hexahedron is shown in Figure 5a., and the Mosaic Poly-Hexcore mesh with surface poly, poly-prism, transition polyhedron and the bulk hexahedron are shown in Figure 5b.

Similarly, Figure 6. shows a volume mesh on the cut plane intersecting the slat and the wing. The ANSYS Fluent meshing tool generously grows prisms from the surfaces using a uniform prism generation method and avoids any intersection between the prism layers in the proximity by keeping a user specified number of volume elements. Figure 6a & Figure 6b shows Hexcore and Poly-hexcore volume mesh respectively.

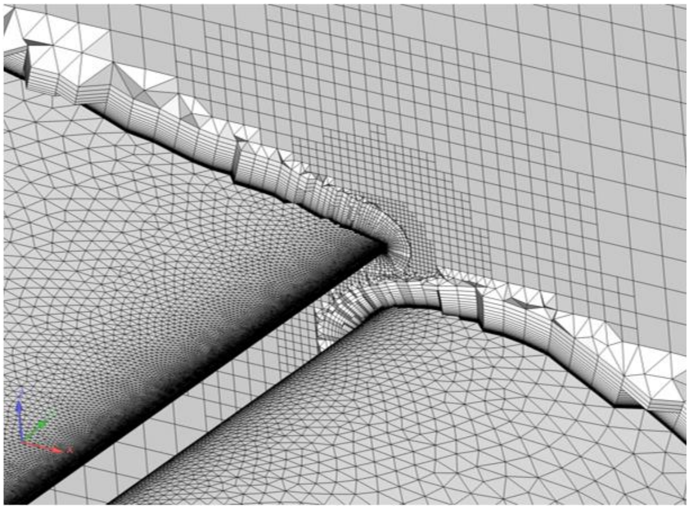

(a)

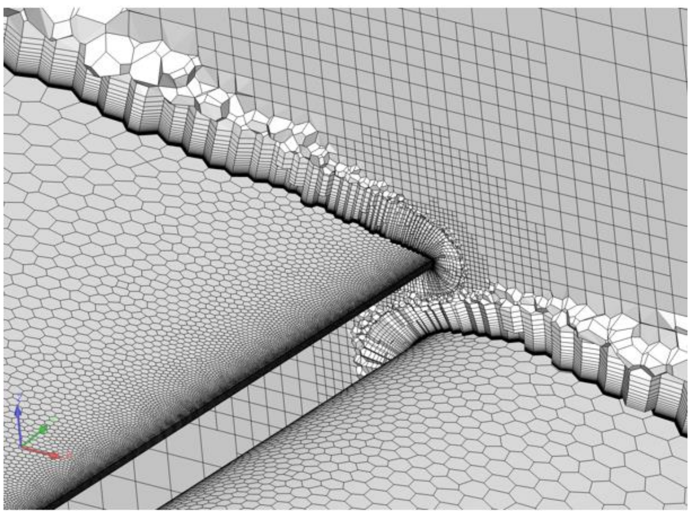

(b)

Figure 5. JSM-WBNP, Surface & Volume mesh, (a) Hexcore, (b) Mosaic Poly-Hexcore.

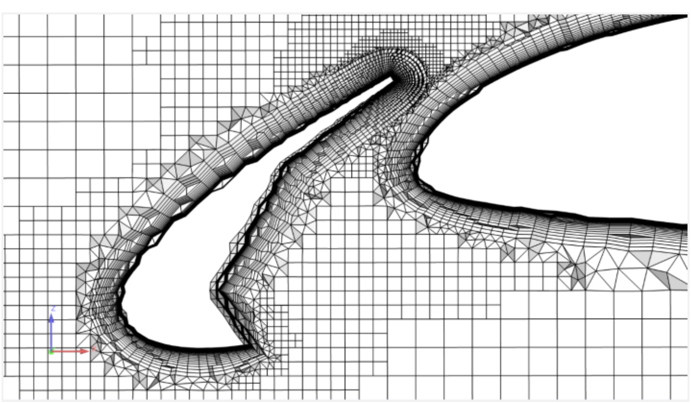

(a)

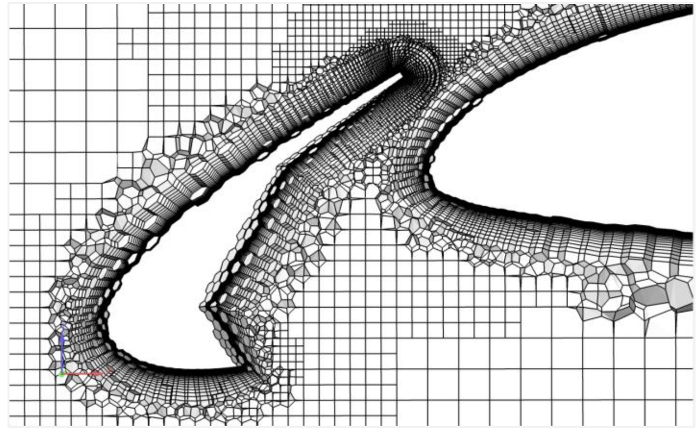

(b)

Figure 6. JSM-WBNP, Volume mesh, (a) Hexcore, (b) Mosaic Poly-Hexcore.

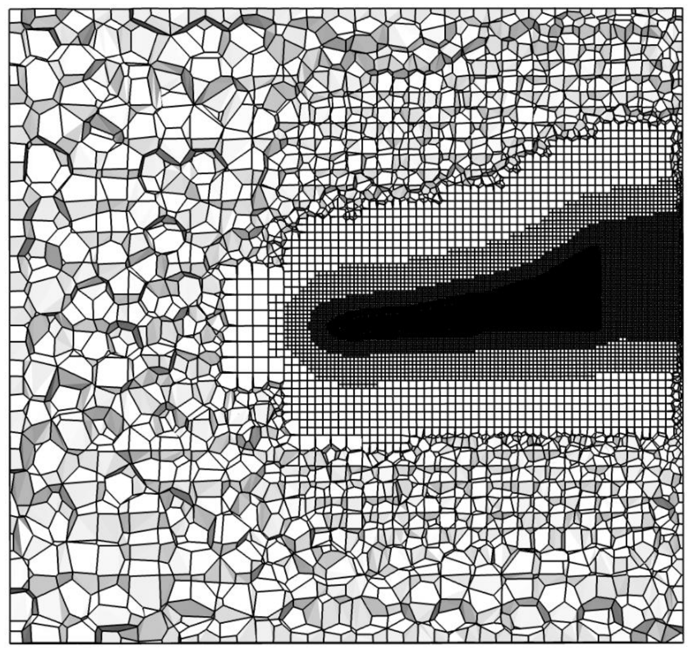

(a)

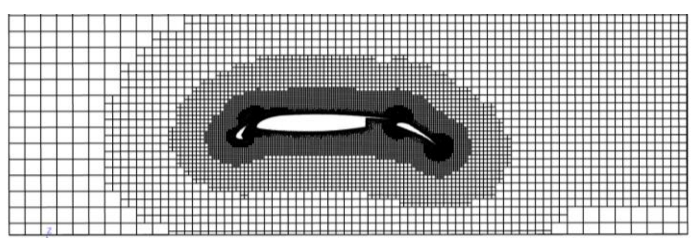

(b)

Figure 7. JSM-WBNP, Mosaic Poly-Hexcore mesh, (a) Wake refinement (b) Surface off-set refinement.

Figure 7. shows a volume mesh refinement in the wakes and the near field surface off-set regions. Figure 7a. captures the wake

refinement zone extended up to the outlet boundary, which is important in order to predict pressure drag accurately. Figure 7b. captures an off-set refinement on the intersecting plane over the slat, wing and flap, illustrating a proper transition between the refinement element sizes from the surface into the volume. These refinements are important to accurately predict complex flow phenomenon, such as the boundary layer transition, primary and secondary vortex interactions, turbulent wake boundary layer interactions, etc.

A detailed mesh sizes comparison between the Hexcore and the Mosaic Poly-Hexcore mesh is illustrated in Table 2. The total number of boundary prism layers *"41"*, first prism layer height *"Δy=0.00242"* and the uniform growth rate *"1.16"* is kept consistent between both the meshes. As mentioned previously, the Mosaic Poly-Hexcore mesh resulted in a *~48%* reduced total element count compared to the conventional Hexcore, capturing all the geometric and the bulk region details. This significant reduction in the total element count is due to reduction in the transition and the boundary layered region elements. The transition elements between the layered boundary prism and the bulk hexahedron shows a *~70%* reduction, for the Mosaic polyhedron compared to the tetrahedron elements. Similarly, the boundary layered poly-prism mesh showed a *~47%* reduction, compared to the wedge-prism of the Hexcore mesh. There also a, *~17%* reduction in the bulk hexahedron number with the Mosaic Poly-Hexcore compared to the Hexcore mesh, which is due to the removal of one hexahedron layer close to the boundary to allow better connection between polyhedron and hexahedron elements.

Table 2. JSM-WBNP mesh details.

Mesh Type	Total Prism layers	wall Δy (mm)	Total Elements	**%Less** *Total Elements*	Transition *(Tet/poly)*	**%Less** *Transition*
Hexcore	41	0.00242	233,066,868		20,298,237	
Poly-hexcore	41	0.00242	121,347,843	**-48%**	6,112,848	**-70%**

Bulk Hexahedron	**%Less** *Hexahedron*	Boundary faces	**%Less** *Boundary faces*	Boundary layered *(wedge/poly)* prisms	**%Less** *Prisms*
11,385,815		12,601,274		201,382,816	
9,444,294	**-17%**	5,246,522	**-58%**	105,790,701	**-47%**

Table 3. Mosaic Poly-Hexcore mesh parallel scalability.

Mesh Type	#Cores	Mesh Time (Minutes)	Speed *(Million elements/ Minute)*	Peak Memory/ core (GB)	Total Peak Memory (GB)	Total Element *(million)*
poly-hexcore	1	1639	0.07	112	112	121
	32	246	0.50	6	180	121

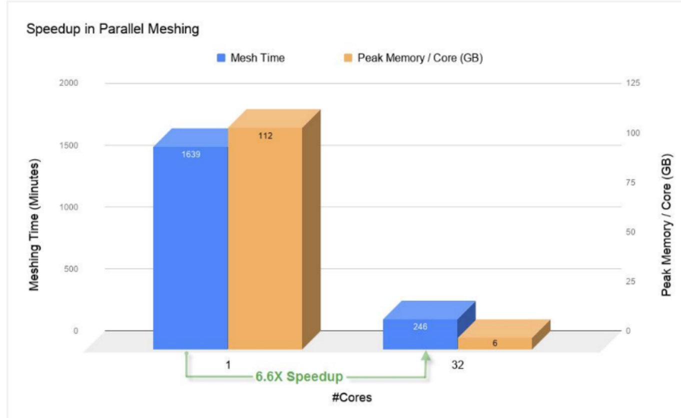

Figure 7. JSM-WBNP, Mosaic Poly-Hexcore parallel scalability.

Furthermore, the Mosaic Poly-Hexcore mesh can be parallel scalable on the high-performance computing (HPC) platform. For example, on a multi-core machine *(CPU: 2x Intel(R) Xeon(R) Gold 6142 CPU @ 2.60GHz, RAM: 192GB (6GB/core)),* an approximately *121* million element mesh is generated *6.6* times faster, on 32 cores compared to the serial core. Similarly, the serial compute core machine memory *(RAM)* requirements can be relaxed, by the distributed meshing processes on the multiple machines acquiring *6 GB* memory per core. Table 3. illustrates the Mosaic Poly-Hexcore parallel scalability details and Figure 7. shows the graphical representation of parallel meshing speedup and per core RAM consumption.

FLOW PARAMETERS AND SOLVER NUMERICS

The wind tunnel flow parameters are outlined in Table 4. including the flow Mach number and the angles of attack (α) sweep. For CFD, all simulations are "free air", and no wind tunnel walls, or model support systems are included.

The steady-state RANS simulations are performed with ANSYS Fluent R19.2, a cell-centered finite volume solver. A pressure-based fully coupled algorithm is employed with second order upwind and central discretization methods for convective and diffusion terms, respectively. The resulting discrete linear system is solved using a point implicit (Gauss-Seidel) linear equation solver in conjunction with an algebraic multigrid (AMG) method. Turbulence is modelled using the k-ω Shear Stress Transport (SST)[10,11] model, while transition is modeled using the two-equation SST-Transition model (γ-Reθ)[12]. Additionally, the models' constant *a1* is modified from 0.31 *(default)* to 1, to better represent the separated and adverse pressure gradient flows[13]. However, further investigation indicates that the early flow separation observed with the default *a1* constant can be corrected by switching from steady to unsteady RANS simulations. This will be covered in the separate paper.

Table 4. JSM-WBNP simulation parameters.

Mach Number	0.172
Alphas	4.36, 10.47, 14.54, 18.58, 20.59, and 21.57^0
Reynolds Number based on MAC	1.93 million
Reference Static Temperature	551.79^{0}R (=33.40^{0}C=92.12^{0}F)
Reference Static Pressure	747.70 mmHg (=14.458 PSI)
Mean Aerodynamic Chord (MCA)	529.2 mm **model scale**
Important Details:	• All simulations are "free air"; no wind tunnel walls or model support systems.

RESULTS AND DISCUSSIONS

In this section, the results obtained on the JSM-WBNP in nominal landing configuration with high lift devices deployed are compared and discussed between CFD *(Mosaic Poly-Hexcore & Hexcore mesh)* and the wind tunnel measurements.

Figure 8. shows the C_L-α, C_D-α, C_L-C_D and C_L-C_M plot comparisons for JSM-WBNP with experimental data. Both the computational results with Transition-SST $a1=1$ and SST $a1=1$ on Mosaic Poly-Hexcore and Hexcore mesh show good agreement with the experimental data at $\alpha=18.58^0$ and below. Both the Transition-SST $a1=1$ and SST $a1=1$ turbulence model predicts the linear portion of the C_L-α curve accurately and matches within *~2%* error of the experimental data on both the meshes. However, the non-linear portion of the C_L-α curve is better predicted by the Transition-SST $a1=1$ compared to the SST $a1=1$ model. Furthermore, the accuracy of after-stall results ($\alpha=20.58^0$ and $\alpha=21.57^0$) are questionable with steady-state RANS calculations, due to highly separated flow behavior, thus the unsteady RANS investigations are ongoing and will be presented in a separate paper.

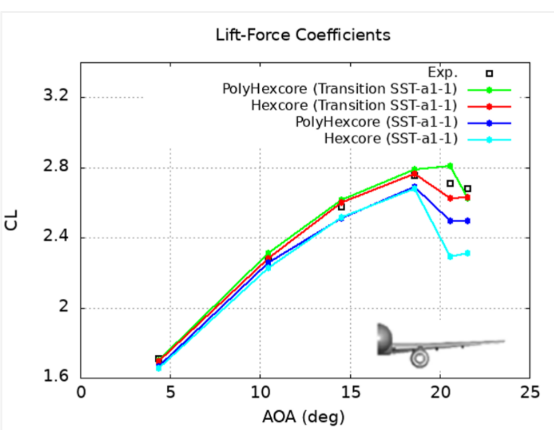

(a)

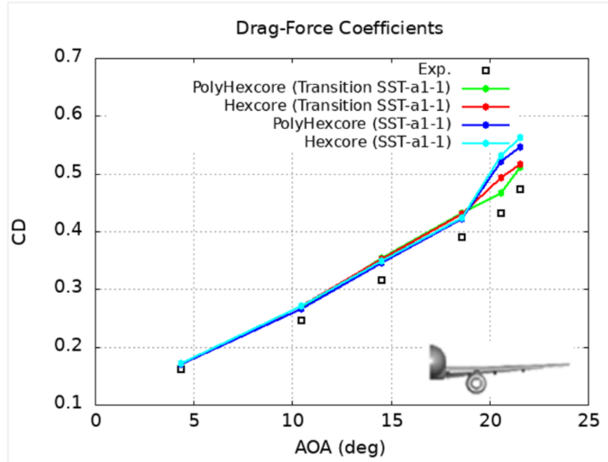

(b)

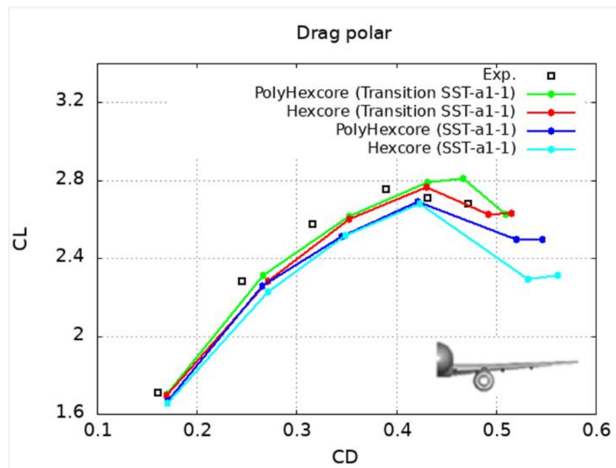

(c)

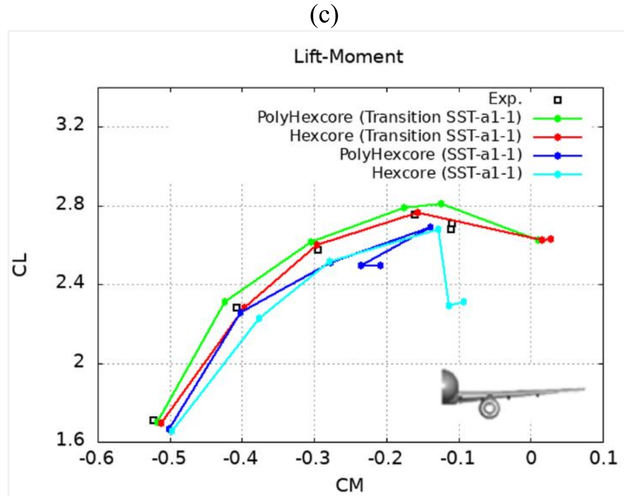

(d)

Figure 8. JSM-WBNP, Aerodynamic Coefficients, (a) Lift Curve *(C_L vs α)*, (b) Drag curve *(C_D vs α)*, (c) Drag Polar *(C_L vs C_D)*, (d) Lift-Moment curve *(C_L vs C_M)*

The differences in drag between the two models and the meshes are generally very close *(see Figure 8b)*. However, both C_D-α, and C_L-C_D plots show more differences between the wind tunnel and computational results, with a *~8-40* drag counts difference between the computational and the experimental data, *(for more speculations related to increase in computational drag please read through reference 2 & 3)*. These differences will be further investigate based on the unsteady RANS simulations, mesh refinements and the improved solver numerics, which are out of scope for this paper. Similarly, the C_L-C_M plot *(see Figure 8d)* shows, that the nose down pitching moment is lower for SST *a1=1* model than the Transition-SST *a1=1* model for both meshes, with the latter being close to the experiments at $\alpha=18.58^0$ and below. However, the after-stall results are questionable and are under investigations.

Furthermore, to perform close comparisons between the Mosaic Poly-Hexcore and Hexcore mesh to identify benefit/advantage of one over the other, which is the main objective of this paper, a critical angle of attack $\alpha=18.58^0$ and Transition-SST *a1=1* model is chosen.

Table 5. illustrates the ANSYS Fluent R19.2 solver time statistics between both the meshes. The Hexcore mesh with *233million* elements takes *5.25hrs* and *10500hrs* Wall-clock and CPU time respectively, to complete *2500-iterations* on *2000-CPUs* of a CRAY XC40 Supercomputer. Whereas, the Mosaic Poly-Hexcore mesh with *121million* elements, takes *3.11hrs* and *62200hrs*, for the same number of iterations and CPUs, which is approximately *41%* less compared to the Hexcore mesh. Figure 9. shows lift force C_L monitor plots. As can be seen, C_L reaches a constant level within *500-1000-iterations* for both the meshes. Next, comparing averaged C_L over the last *1000-iterations* between the meshes shows a difference of only *1.1%*. However, comparing this difference with the experimental $C_{L\text{-}Exp.}=2.75$, shows, Poly-Hexcore and Hexcore predict *~1.5%* and *~0.4%* higher lift respectively.

Hence, the Mosaic Poly-Hexcore mesh shows clear benefits from the solver performance point of view, however, even though the error in C_L predictions is well within acceptable limits considering the wind tunnel measurement uncertainties, further accuracy is confirmed by comparing C_p at spanwise locations, surface flow visualizations, china-clay boundary layer transitions between computational results from both the meshes and the experimental measurements. Furthermore, the eddy viscosity ratios at multiple cut planes in x-direction and z-directions are compared to check the consistency of turbulent wake flow behavior in the bulk region over the wing, nacelle-pylon and the high-lift devices between both the meshes.

Table 5. JSM-WBNP, solver time statistics for $\alpha=18.58^0$.

Mesh Type	Total Elements (million)	#Iteration	#Cores	Solver time (hr)	**%Less Solver time**	CPU Time (hr)	**C_L**
Hexcore	233	2500	2000	5.25		10500	**2.76**
Poly-Hexcore	121	2500	2000	3.11	**-41%**	6220	**2.79**

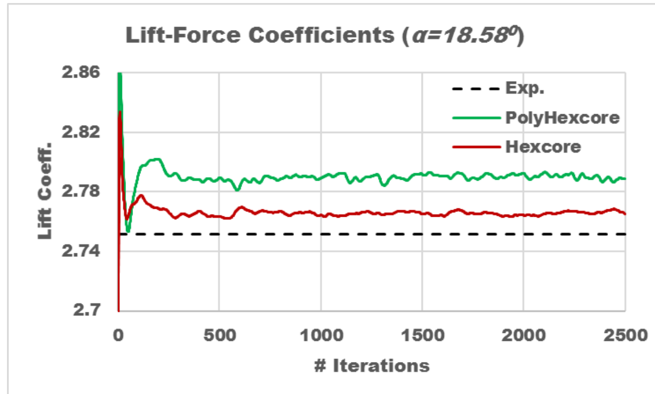

Figure 9. JSM-WBNP, Lift coefficient monitor convergence.

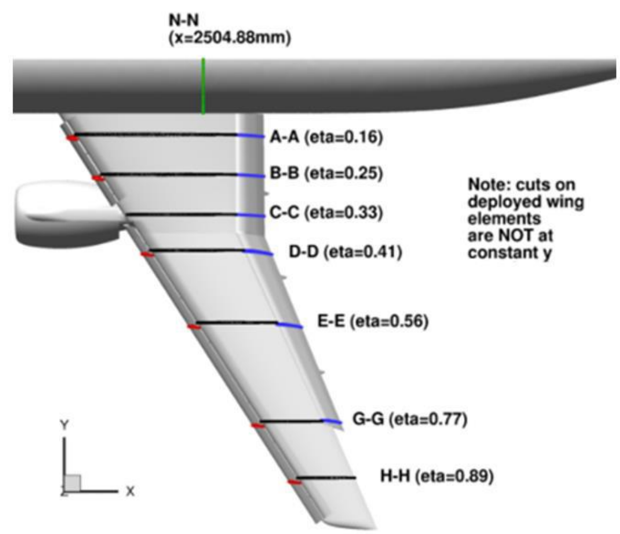

Figure 10. JSM-WBNP, Wing C_p. extraction stations.

Experimental C_p extraction locations along the wingspan are shown in Figure 10. Computational C_p predicted for $\alpha=18.58^0$ and the Transition-SST *a1=1* model along the wingspan, shows a very good match between the Mosaic Poly-Hexcore and Hexcore mesh. Both the meshes show excellent agreement with the experimental C_p over slat, wing and flap up to the location *G-G (eta=0.77)* from the wing-root. However, the location *H-H (eta=0.89)* near wing-tip shows an increase in C_p on the suction side due to unresolved separated flow, as seen in Figure 11.

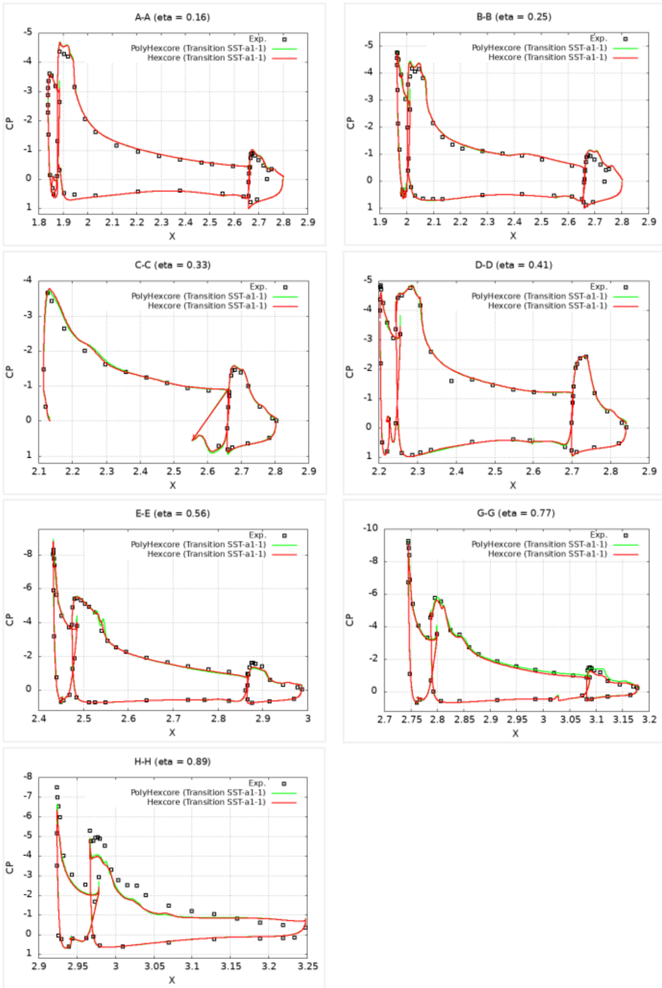

Figure 11. JSM-WBNP, C_p plots comparison with experimental measurements $\alpha = 18.58^0$.

Figure 12a. shows the wind tunnel oil flow visualization image, illustrating the surface flow pattern over the nacelle-pylon, slat, wing and flap. In addition, Figure 12b & Figure 12c show computational surface streamlines colored by skin-friction coefficient for the Mosaic Poly-Hexcore and Hexcore meshes respectively. The effect of slat bracket wakes can be clearly seen over the wing surface in both the computational and experimental results. Furthermore, a small spiral vortex initially seen at lower "*α*" at the outboard wing leading edge has grown in strength with increase in *"α"* and interact with the outermost slat support bracket turbulent wake, which at $\alpha = 18.58^0$ resulted in a slightly bigger separation region as compared to the experiments. This effect was observed in the C_p plot at location *H-H (eta=0.89)*, which showed an increase in C_p on the suction side. For further insight into surface flow visualizations and wing spanwise *Cp* comparisons between computations and experiments for the complete angle of attack sweep, please see references 2 & 3.

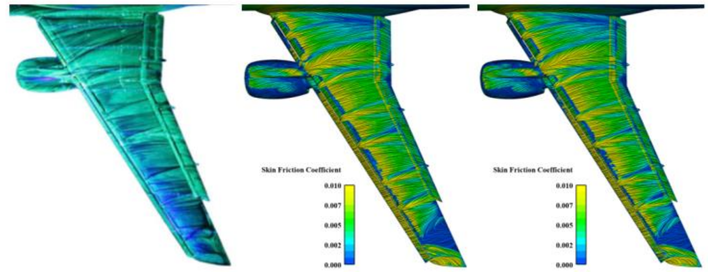

(a) (b) (c)

Figure 12. JSM-WBNP, Experimental oil flows *vs*. CFD surface flow pattern, Transition-SST $a1=1$, $\alpha=18.58^0$ (a) Exp. Oil flow, (b) Mosaic Poly-Hexcore mesh, (c) Hexcore mesh.

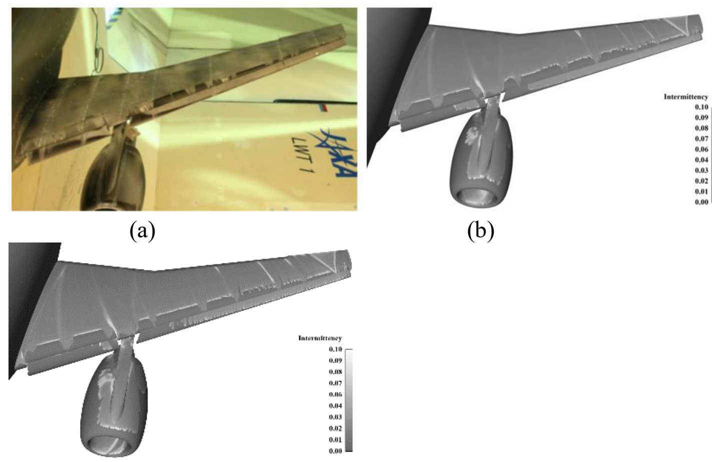

(a) (b)

(c)

Figure 13. JSM-WBNP, Boundary layer transition visualization, experimental china-clay and CFD Intermittency, Transition-SST $a1=1$, $\alpha=18.58^0$, (a) Exp. China-clay, (b) Mosiac Poly-Hexcore mesh, (c) Hexcore mesh.

The wind tunnel china-clay visualization image highlighting laminar to turbulent flow transition is compared with the computational intermittency contour *(see Figure 13)*. Overall the computational flow transition shows good agreement with the experimental visualization. However, on the inboard slat region close to the fuselage, computations predominately indicate laminar flow, whereas the experiment indicates laminar-turbulent transition at slat trailing edge. This anomaly will be further investigated by fulfilling transition prediction mesh requirements, by improving mesh in these key regions with additional BOIs.

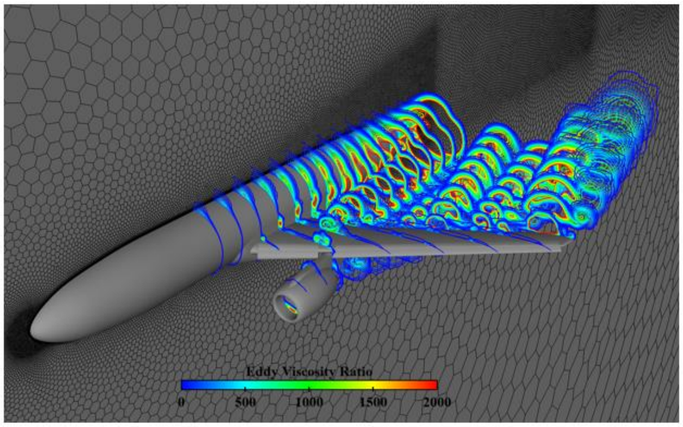

(a)

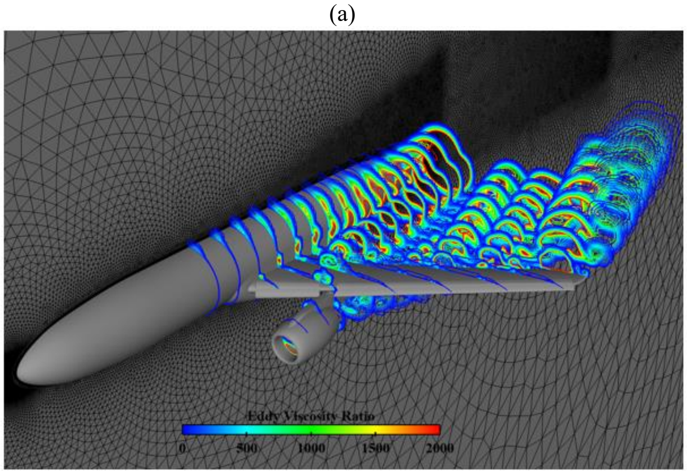

(b)

Figure 14. JSM-WBNP, Eddy viscosity ratio contour in y-z planes, Transition-SST *a1=1,* α=*18.58⁰*, (a) Mosiac Poly-Hexcore mesh, (b) Hexcore mesh.

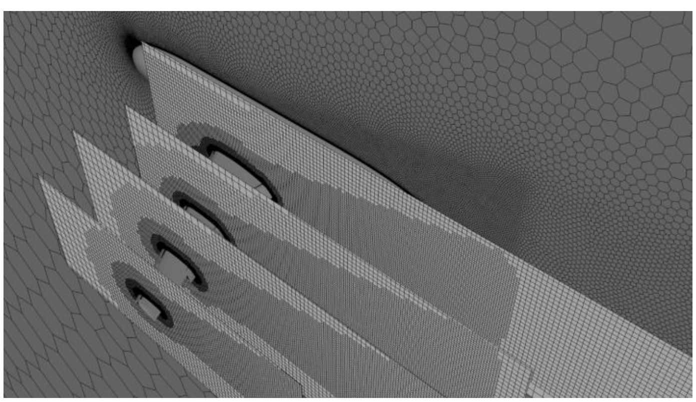

(a)

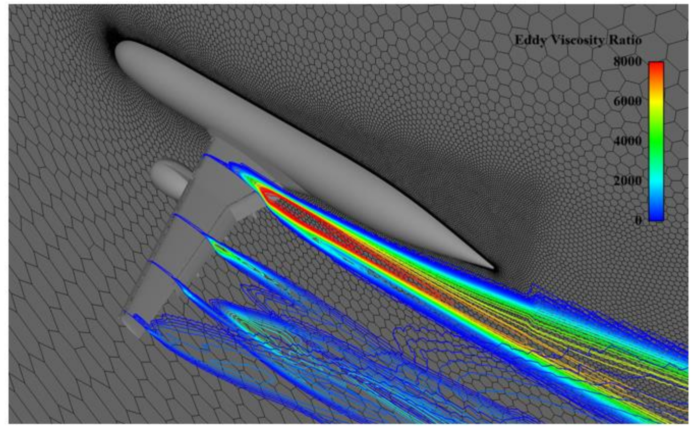

(a)

Figure 15. JSM-WBNP, Eddy viscosity ratio contour in x-y planes, Transition-SST *a1=1,* α=*18.58⁰*, (a) Mosaic Poly-Hexcore bulk region mesh along the wingspan locations, (b) Mosaic Poly-Hexcore eddy viscosity ratio contours along the wingspan locations.

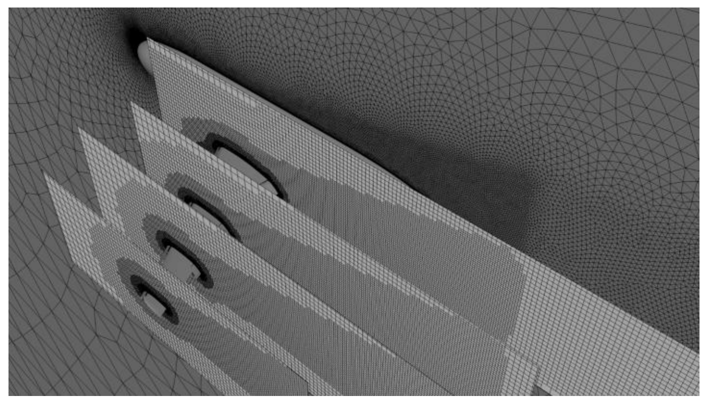

(a)

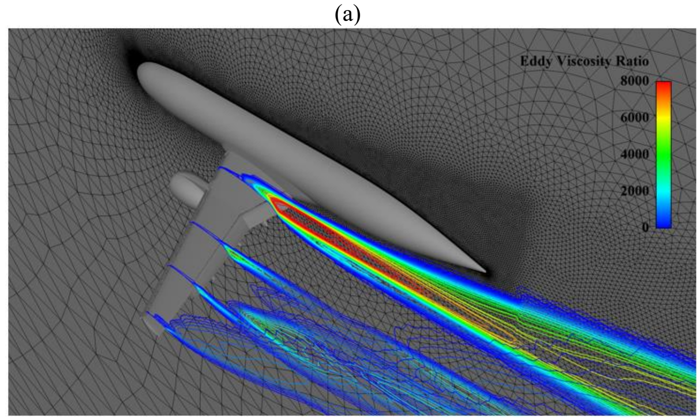

(b)

Figure 16. JSM-WBNP, Eddy viscosity ratio contour in x-y planes, Transition-SST *a1=1,* α=*18.58⁰*, (a) Hexcore bulk region mesh along the wingspan locations, (b) Hexcore eddy viscosity ratio contours along the wingspan locations.

Figure 14., Figure 15., and Figure 16. show eddy viscosity ratio contours on the multiple spanwise locations. The purpose of this comparison is to illustrate the consistency in the turbulent wake prediction between the Mosaic Poly-Hexcore and the Hexcore mesh. Figure 14a. & Figure 14b. show an identical spiral vortex originating from the wing-fuselage intersection, traveling downstream and combining with other vortices from the fuselage top, engine pylon and FTFs to form a bigger vortex moving inboard close to the fuselage tail. Similarly, other vortices originating from the wingtip, outboard flap fairings and support brackets are identical between both meshes. However, there is a small difference observed in the wake behind the engine nacelle with the Hexcore mesh, which shows a more diffuse vortex, compare to the Mosaic Poly-Hexcore mesh. Figure 15b. & Figure 16b. indicate very similar eddy viscosity ratio contours on the multiple cut planes along the wingspan direction between the Mosaic Poly-Hexcore and Hexcore mesh, respectively. The reason being the constant element size octree hexahedral mesh in the bulk region, as shown in Figure 15a. and Figure 16a. respectively.

CONCLUSION

The Mosaic meshing technology to predict complex high-lift aerodynamics on a typical 100-passenger class regional jet airliner in a nominal landing configuration is validated against wind tunnel measurements and compared also against the conventional Hexcore mesh to highlight the benefits and/or advantages for solver performance and result accuracy.

The Mosaic meshing technology is parallel scalable. For example, on *32* parallel compute cores *(CPU: 2x Intel(R) Xeon(R) Gold 6142 CPU @ 2.60GHz, RAM: 192GB (6GB/core)),* a *121 million* element mesh parallel execution is *6.6* times faster, than serial. Furthermore, compared to the conventional Hexcore with tetrahedron elements between wedge-prism and the bulk hexahedron, the Mosaic Poly-Hexcore with general polyhedron elements between the poly-prism and the bulk hexahedron resulted into a *~48%* reduction in the total element count, which consequently speeds up the ANSYS Fluent R19.2 flow solver by *~41%.*

Comparing the averaged C_L over the last *1000-iterations*, for $\alpha=18.58^0$ and the Transition-SST *a1=1* model, shows a difference of only *1.1%* between both the meshes. However, comparing this difference with experimental $C_{L\text{-}Exp.}=2.75$ shows Poly-Hexcore and Hexcore predict *~1.5%* and *~0.4%* higher lift respectively, which is well within the acceptable limits considering the wind tunnel measurement uncertainties. Further, the averaged C_D shows a very similar value between both the meshes, however, compared to wind tunnel measurement shows a *~10%* increase in drag *(for more speculations related to increase in computational drag please read through reference 2 & 3)*.

Computational C_p predicted along the wingspan for $\alpha=18.58^0$ and the Transition-SST *a1=1* model, shows an almost exact match between the Mosaic Poly-Hexcore and Hexcore mesh. Both predictions show excellent agreement with the experimental C_p over slat, wing and flap up to the measuring location *G-G (eta=0.77)* from the wing-root. However, the location *H-H (eta=0.89)* near the wingtip shows an increase in C_p on the suction side due to unresolved separated flow.

The experimental oil flow visualization illustrating the surface flow patterns and china-clay visualization highlighting the transition from laminar to turbulent are captured nicely by both the meshes, for $\alpha=18.58^0$ and Transition-SST *a1=1* model.

The overall comparison between the Mosaic Poly-Hexcore and Hexcore mesh indicates that the Mosaic Poly-Hexcore provides an advantage in the solver performance. The results accuracy can be further improved by investing saved mesh elements in the critical flow regions, which makes Mosaic Poly-Hexcore a best choice for future computations.

Future work includes, unsteady RANS simulations to understand the default SST *a1* constant impact on correcting unresolved flow separation and the after stall separated flow behavior.

ACKNOWLEDGMENTS

The authors would like to thank the HiLiftPW3 organizing team for providing rich data for the CFD solver comparisons. Also, the authors would like to thank David Whitaker from CRAY for his support, and generously recognize CRAY HPC for providing computational resources for performing these simulations. Many thanks to John Stokes, Shoaib Shah, Patrick Sharkey, Florian Menter and Boris Makarov, all from ANSYS, for their valuable inputs and support. Special thanks to Vinod Mahale and Andy Wade, from ANSYS, for their assistance during Mosaic Poly-Hexcore mesh generation.

Fluent Scalability on CRAY XC Series Supercomputers

The Cray XC system offers excellent parallel performance for ANSYS Fluent, with continued scaling to more than 2,000 cores for ~121 and ~233-million-cell Mosaic Poly-Hexcore and Hexcore simulations respectively, as seen in Figure 17. Cray and ANSYS are committed to delivering high performance computing capabilities that quickly bring aerospace applications to new heights of simulation fidelity. This project is just one example of how ANSYS and Cray collaborate to build robust solutions for a broad set of engineering simulations.

Cray XC40 system combines the advantages of its Aries™ interconnect and Dragonfly network topology, Intel® Xeon® processors, integrated storage solutions, and major enhancements to the Cray Linux® Environment and programming environment. The Cray XC40 supercomputer is a groundbreaking architecture upgradable to 100 petaflops per system.

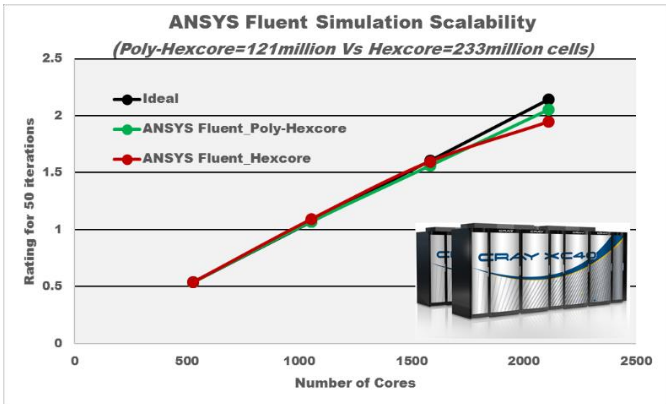

Figure 17. Performance chart of ANSYS Fluent Simulation on CRAY XC40 Supercomputers.

REFERENCES

1. 3rd AIAA CFD High Lift Prediction Workshop, URL: http://hiliftpw.larc.nasa.gov/,email: hiliftpw@gmail.com, June 2015.
2. Zore, K., Shah, S., Stokes, J., Sasanapuri, B., Sharkey, P. "*ANSYS CFD Study for High-Lift Aircraft Configurations*", AIAA Applied Aerodynamics Conference, 25 - 29 June 2018, Atlanta, GA. AIAA 2018-2844.
3. Zore, K., Shah, S., Stokes, J., Sasanapuri, B., Sharkey, P., *"ANSYS CFD Validation for Civil Transport Aircraft in High- Lift Configuration Part-1"* Tenth International Conference on Computational Fluid Dynamics (ICCFD10), Barcelona, Spain, July 9-13, 2018. ICCFD10-071.
4. Rumsey, C., Slotnick, J., Long, M., Stuever, R., Wayman, T., "*Summary of the First AIAA CFD High-Lift Prediction Workshop*," Journal of Aircraft, Vol. 48, No. 6, pp. 2068-2079, November-December 2011.
5. Ito, T., Ura, H., Yokokawa, Y., Kato, H., Mitsuo, K., and Yamamoto, K., *"Experimental and CFD of a High-Lift Configuration Civil Transport Aircraft Model,"* AIAA Paper 2006-3452, June 2006.
6. Christopher L. Rumsey and Jeffrey P. Slotnick. *"Overview and Summary of the Second AIAA High-Lift Prediction Workshop"*, Journal of Aircraft, Vol. 52, No. 4 (2015), pp. 1006-1025
7. Mitsuhiro Murayama, Yuzuru Yokokawa, Kazuomi Yamamoto, and Yoshine Ueda. *"CFD Validation Study for a High-Lift Configuration of a Civil Aircraft Model",* 25th AIAA Applied Aerodynamics Conference, 25 - 28 June 2007, Miami, FL
8. Zore, K., Caridi, D., Lockley, I., *"Fast and Accurate Prediction of Vehicle Aerodynamics using ANSYS Mosaic Mesh".* SAE COMVEC™ September 9-11, 2019, Indianapolis, IN USA. Submitted.
9. ANSYS Fluent Mosaic Technology Automatically Combines Disparate Meshes with Polyhedral Elements for Fast, Accurate Flow Resolution, https://www.ansys.com/products/fluids/ansysfluent/mosaic-meshing-technology.
10. Menter, F. R., *"Two-Equation Eddy-Viscosity Turbulence Models for Engineering Applications,"* AIAA Journal, Vol. 32, No. 8, pp. 1598-1605, (1994).
11. Menter, F. R., Kuntz, M., and Langtry, R., *"Ten Years of Industrial Experience with the SST Turbulence Model,"* Turbulence, Heat and Mass Transfer 4, ed: K. Hanjalic, Y. Nagano, and M. Tummers, Begell House, Inc., 2003, pp. 625 - 632.
12. Langtry, R. B. and Menter, F. R., *"Correlation-Based Transition Modeling for Unstructured Parallelized Computational Fluid Dynamics Codes,"* AIAA Journal, Vol. 47, No. 12, December 2009, pp. 2894-2906.
13. Hiroshi Kato, Keiichi Ishiko, and Akira Yoshizawa. *"Optimization of Parameter Values in the Turbulence Model Aided by Data Assimilation"*, AIAA Journal, Vol. 54, No. 5 (2016), pp. 1512-1523.